bandnotch is present at 4.22 GHz, at 30 dB rejection, while the other bandnotch is absent. State 4 is reverse: with a bandnotch at 3.51 GHz, at 37 dB loss, only. The passband insertion loss varies between 0.32 dB in state 3 and 0.48 dB in state 4.

3.3. S-Parameters with PIN Diodes

In the fabricated structure with PIN diodes, Agilent E8361A PNA Network Analyser was used to carry out the measurements of the S-parameters. The results are presented in Figure 5(a) for state 1 and in Figure 5(b) for state 2. In state 1, no bandnotch exists and the 3 dB passband is from 3.14–5.35 GHz. The filter's insertion loss is roughly 0.2 dB. In state 2, the passband is 3.19–5.15 GHz. As also seen in the passband, dual bandnotch are introduced. The obtained rejection at these dual bandnotch is 5 dB less than the one achieved by the Graphene based switches, i.e. at 25 dB. Furthermore, the dual bandnotch have moved to frequencies of 3.48 GHz and 4.26 GHz. These shifts are caused by the discrepancies in the fabrication. An insertion loss of 0.8 dB is present in the passband. State 3, presented in Figure 5(c), has a passband of 3.14–5.35 GHz and state 4, shown in Figure 5(d), has a passband of 3.19–5.2 GHz at an insertion loss of 0.4 dB and 0.6 dB respectively. State 3 shows a single bandnotch at 4.28 GHz ($S_{21} = 25.5$ dB) while state 4 has one at 3.48 GHz ($S_{21} = 25$ dB) only.

3.4. Measured Linearity With PIN Diodes

The nonlinearity introduced by a PIN diode is a function from Eq. (4) of the forward bias current I_F and the RF current i_f. Generally, better linearity may be obtained when the extent of the bias current modulation by the RF current decreases. The modulation effect can be minimized by deliberately operating at a high forward bias current [11].

For the purpose of validating the high linearity characteristics, the filter was gauged by means of a 5 MHz QPSK signal with and without the PIN diodes. Input power between a range of −25 dBm and 10 dBm resulted in very good linearity. The performance at various passband frequencies in state 1 and state 2 was measured and has been shown in Figure 6.

3.5. Comparison with Other Works

Table 2 presents a comparison of others works in which similar filters were developed.

4. CONCLUSION

A highly linear reconfigurable UWB filter, coupled with two resonators implemented with switches - PIN diodes and Graphene based - is presented. The switches reconfigure the filter between a full bandpass response and a bandpass response with dual bandnotch at 3.5 GHz and 4.2 GHz. The simulation and measurement results of both switching elements in OFF and ON states have been shown. A good agreement is present between the results of the two elements; hence validating the filter concept. These obtained results show no bandnotch in the passband in OFF state; while dual bandnotch are present at 3.5 GHz and 4.2 GHz in ON state. Two further states are also possible when the two resonators are alternated between OFF and ON positions; hence producing their respective bandnotch only. The highly linear nature of the filter has been shown by experimentally evaluating the linearity using a QPSK signal at various passband frequencies of the PIN diodes based filter.

REFERENCES

1. FCC, "Revision of part 15 of the commission's rules regarding ultra-wideband transmission systems," First Note and Order Federal Communications Commission, Washington, DC (2002), 98–153.
2. W. Ahmad and D. Budimir, Reconfigurable WLAN notch for UWB filters, 44th European Microwave Conference (2014) 1536–1539.
3. H. Wang, K.-W. Tam, S.-K. Ho, W. Kang, and W. Wu, Design of ultra-wideband bandpass filters with fixed and reconfigurable notch bands using terminated cross-shaped resonators, IEEE Trans Microw Theory Tech (2014), 1–14.
4. M.F. Karim, Y.-X. Guo, Z.N. Chan, and L.C. Ong, Miniaturized reconfigurable and switchable filter from UWB to 2.4 GHz WLAN using PIN diodes, IEEE MTT-S International Microwave Symposium Digest (2009), 509–512.
5. Y.-H. Chun, H. Shaman, and J.-S. Hong, Switchable embedded notch structure for UWB bandpass filter, IEEE Microw Wireless Component Lett 18 (2008), 590–592.
6. K. Rabbi, L. Athukorala, C. Panagamuwa, J.C. Vardaxoglou, and D. Budimir, Compact UWB bandpass filter with reconfigurable notched band, Electron Lett 49 (2013), 709–711.
7. A.K. Geim and K.S. Novoselov, The rise of graphene, Nat Mater 6 (2007), 183–191.
8. M. Danaeifar, N. Granpayeh, A. Mohammadi, and A. Setayesh, Graphene-based tunable terahertz and infrared band-pass filter, Appl Opt Lett 52 (2013), E68–E72.
9. L. Pierantoni, M. Dragoman, and D. Mencarelli, Analysis of a microwave graphene-based patch antenna, 43rd European Microwave Conference (2013), 381–383.
10. G.W. Hanson, Dyadic green's functions for an anisotropic non-local model of biased graphene, IEEE Trans Antenna Propag 56 (2008), 747–757.
11. W.E. Doherty Jr. and R.D. Joos, PIN diode RF switches, In: The PIN Diode Circuit Designers' Handbook, Watertown: Microsemi Corp., 1998, pp. 18–20.
12. NXP, PIN Diode BAP65–02 Datasheet [Online]. Available at: http://www.nxp.com/documents/data_sheet/BAP65-02.pdf.

DESIGN OF A DUAL-BAND PATCH ANTENNA WITH CIRCULAR PARASITIC ELEMENTS FOR ADAPTIVE POLARIZATION ADJUSTMENT

S. J. Yoo,[1] H. Choo,[1] and G. Byun[2]
[1] School of Electronic and Electrical Engineering, Hongik University, Seoul, Korea
[2] Research Institute of Science and Technology, Hongik University, Seoul, Korea; Corresponding author: kylebyun@gmail.com

Received 9 April 2016

ABSTRACT: *This letter proposes the design of microstrip patch antennas for independent polarization adjustments in two frequency bands. The proposed antenna consists of two radiating patches for dual-band operation, and each patch is composed of a circular resonator and surrounding parasitic elements. The antenna polarization is adaptively adjusted by rotating these parasitic elements for each patch without changing other design parameters. As an evaluation, two sample antennas with linear and circular polarizations are fabricated to measure their radiation characteristics. The results prove that the proposed structure is capable of independent polarization adjustments for dual-band operations.* © 2016 Wiley Periodicals, Inc. Microwave Opt Technol Lett 58:2643–2649, 2016; View this article online at wileyonlinelibrary.com. DOI 10.1002/mop.30112

Key words: *antennas; microstrip antennas; dual-band antennas; antenna polarization*

1. INTRODUCTION

As demand grows for more advanced mobile systems, the integration of multiple antennas has been required for the implementation of various wireless communications systems in a limited space [1–3]. To overcome this spatial constraint, multi-band antennas have been suitable candidates, and a particular antenna polarization is selectively adopted for each frequency band to maintain high reception reliability [4,5]. This reception reliability can be further improved by fine-tuning the antenna polarizations, especially in urban environments, where multipath effects become severe. However, most previous studies have focused only on achieving particular polarizations for specific applications [6–15], which do not provide a tuning capability for antenna polarizations. Although the polarization can be tuned by applying a reconfigurable antenna structure, the design complexity is significantly increased as a result of additional pin diodes with DC bias circuits [16–21]. The design complexity is minimized in Ref. [22], which proposes a flexible polarization adjustment using a single design parameter without any additional components. However, this study is limited to a single frequency band, and the antenna structure should be refabricated to obtain different polarizations.

In this paper, we propose the design of dual-band microstrip patch antennas for an adaptive polarization adjustment in two frequency bands. The proposed antenna has a multi-layer structure with two radiating patches, and each radiating patch consists of a circular resonator and surrounding parasitic elements. These

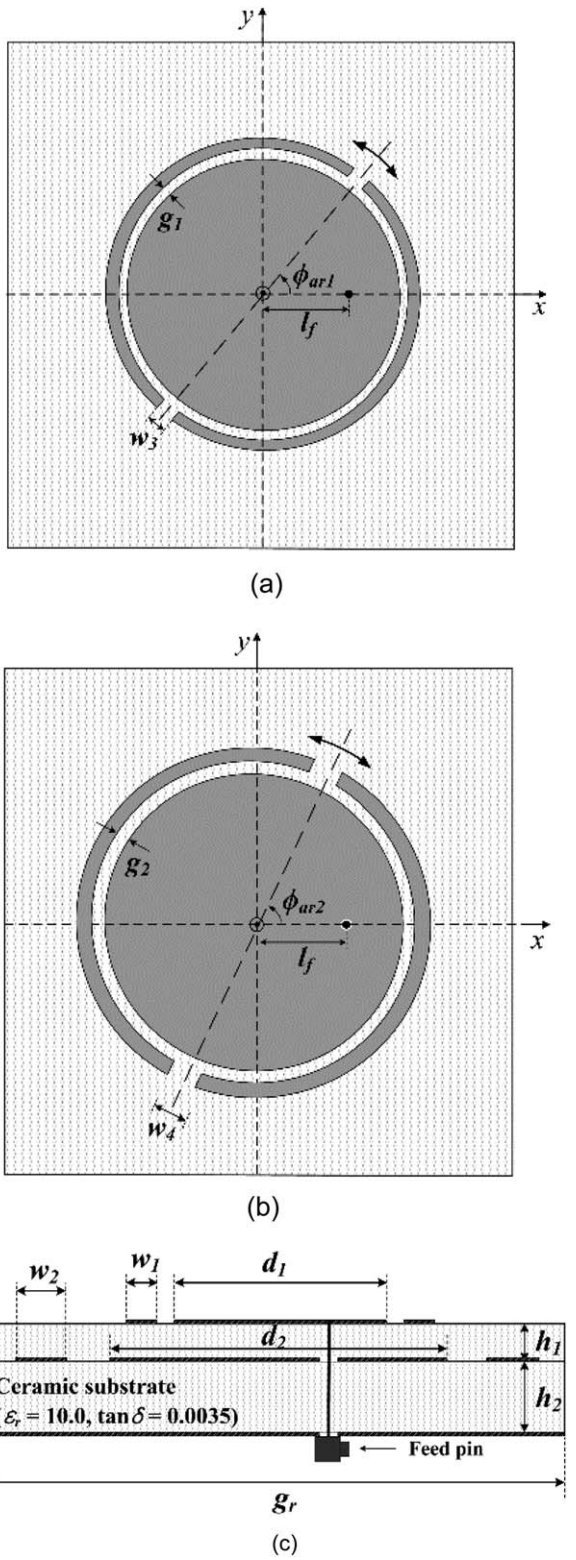

Figure 1 Geometry of the proposed antenna. (a) Top view of upper patch. (b) Top view of lower patch. (c) Side view.

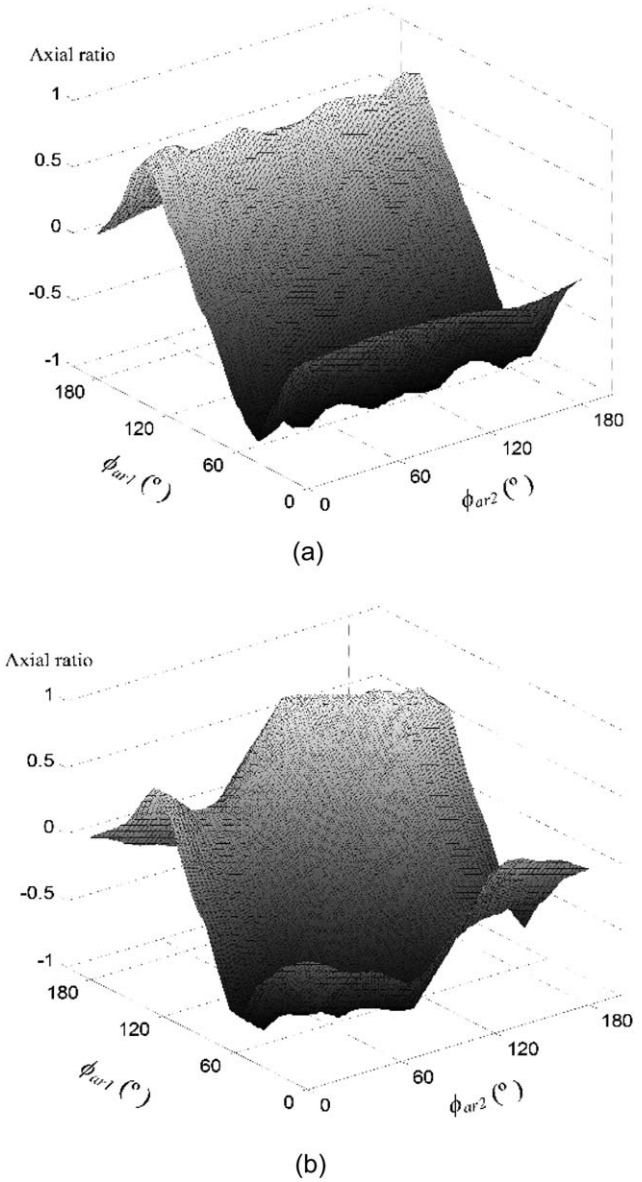

Figure 2 Values of the AR for the angle of the polarizer. (a) Axial ratio at 1.575 GHz. (b) Axial ratio at 1.227 GHz.

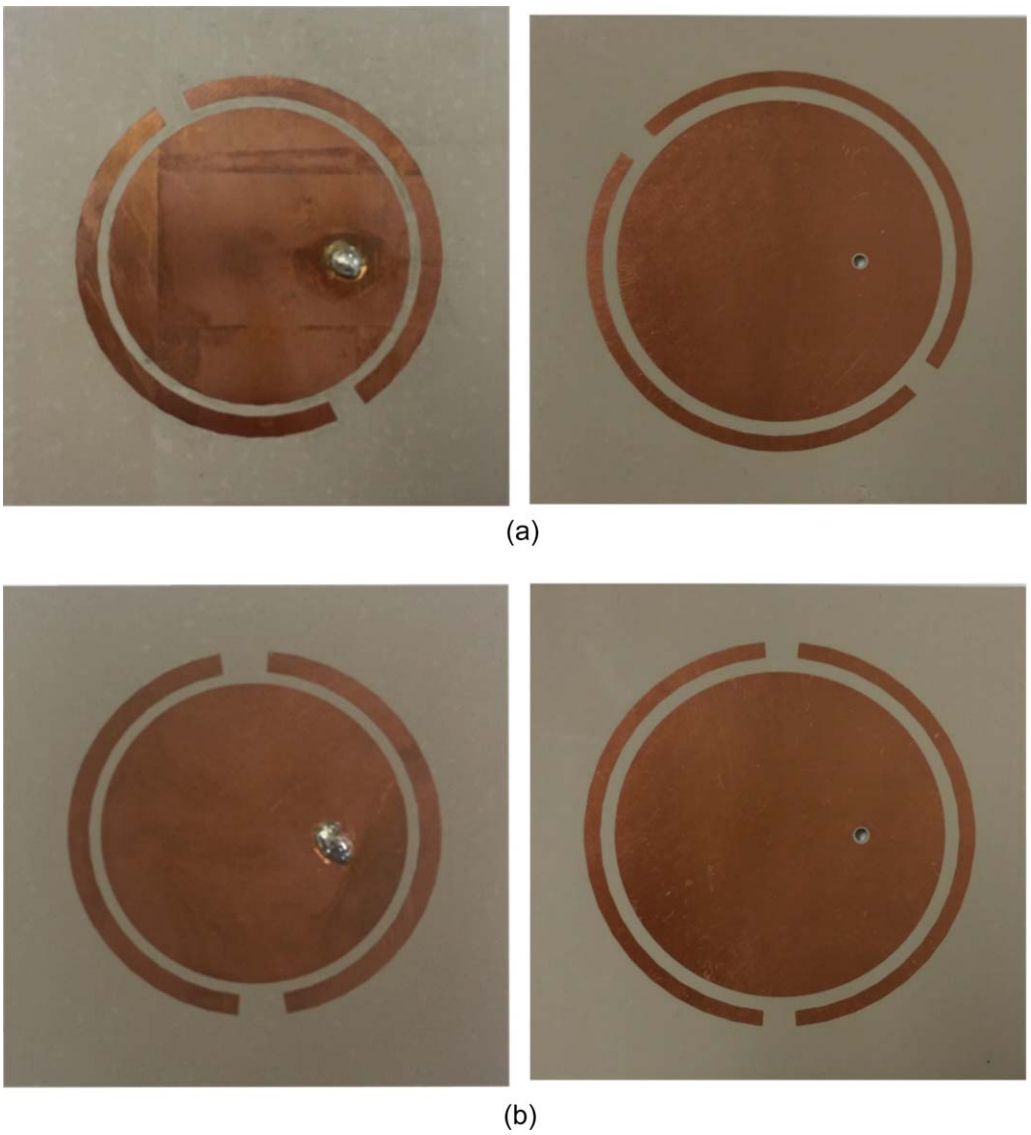

Figure 3 Photographs of the fabricated antennas. (a) Upper and lower patches of circularly polarized antenna. (b) Upper and lower patches of linearly polarized antenna. [Color figure can be viewed in the online issue, which is available at wileyonlinelibrary.com.]

elements are designed to have the circular shape and are simply rotated to independently adjust the antenna polarization for each frequency band across the entire range of the axial ratio (AR). To demonstrate the properties of the dual-band polarization adjustment, two antenna samples with different polarizations are fabricated, and their antenna characteristics are measured in a full anechoic chamber. The magnetic field distributions within patches are further observed in order to demonstrate the capability of the independent polarization adjustment in the two bands. The results show that the proposed antenna is suitable for dual-band polarization adjustments without a significant increase in design complexity.

TABLE 1 Optimized Values of the Proposed Antenna

Parameters	Value
d_1	35.6 mm
d_2	39.2 mm
w_1	1.3 mm
w_2	1.7 mm
w_3	1.9 mm
w_4	2.6 mm
g_1	2.5 mm
g_2	1.9 mm
g_r	60 mm
l_f	9.6 mm
h_1	3.14 mm
h_2	4.71 mm
Substrate	$\varepsilon_r = 10$, $\tan\delta = 0.0035$

2. PROPOSED ANTENNA DESIGN

Figure 1 shows the geometry of the proposed antenna structure, which is capable of an independent polarization adjustment in two frequency bands. The antenna has a multi-layer structure that consists of two circular patches with diameters d_1 and d_2, which are designed to be approximately half the effective wavelength in the operating frequency. Each patch is surrounded by a parasitic element, whose widths are w_1 and w_2, separated into two parts with parameters w_3 and w_4. These parasitic elements are employed to enable the adaptive adjustment of the AR without a frequency shift, as introduced in Ref. 22. In our approach,

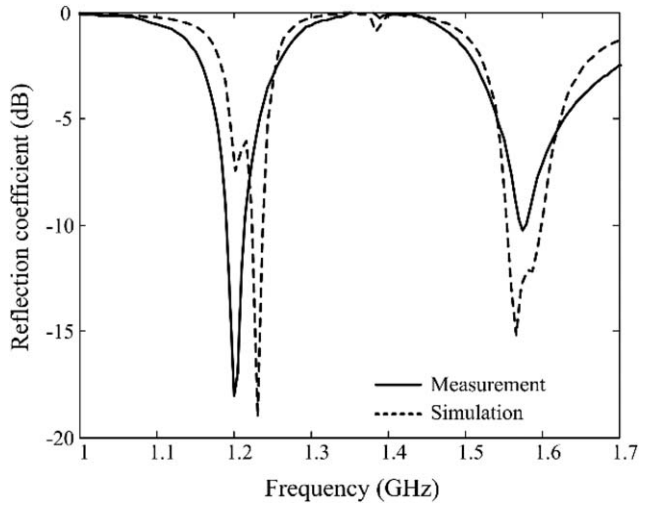

Figure 4 Reflection coefficients of the proposed antenna.

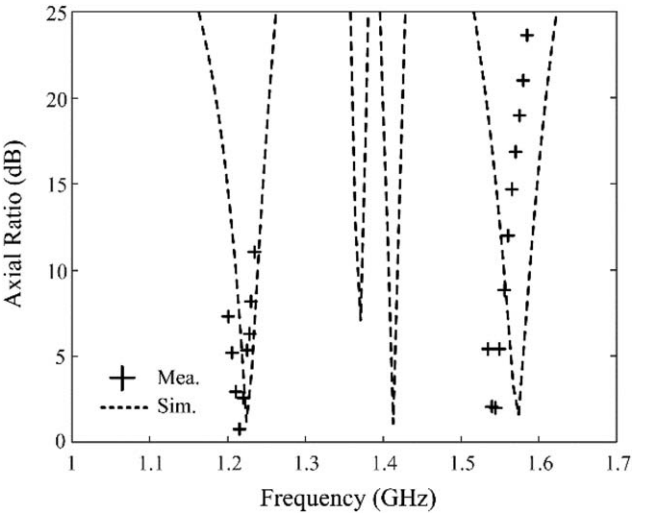

Figure 6 Axial ratio of the proposed antenna.

the parasitic elements are rotated by the parameters ϕ_{ar1} and ϕ_{ar2} to vary the antenna polarization in the two bands independently. The dual-band operation is achieved by feeding the upper patch with a coaxial cable, and the lower patch is electromagnetically coupled to the upper patch. The coupling strength is then controlled by changing the feed position l_f and the substrate heights h_1 and h_2.

Figures 2(a) and 2(b) present variations in AR values at 1.575 GHz and 1.227 GHz, according to the rotating parameters ϕ_{ar1} and ϕ_{ar2}, respectively. Each rotating angle is varied from 0° to 180° at an interval of 10° to observe the AR value at the bore-sight direction. The results show that the proposed antenna can have AR values from −1 to 1, which includes the right-hand circular (RHC), left-hand circular (LHC), linear, and elliptical polarizations in the two frequency bands. For example, the RHC polarization at 1.575 GHz can be obtain when ϕ_{ar1} has an angle between 120° and 130° for any ϕ_{ar2}. Then, the RHC polarization at 1.227 GHz can be achieved when the range of ϕ_{ar2} is from 120° to 140° with a fixed ϕ_{ar1} value of 120°.

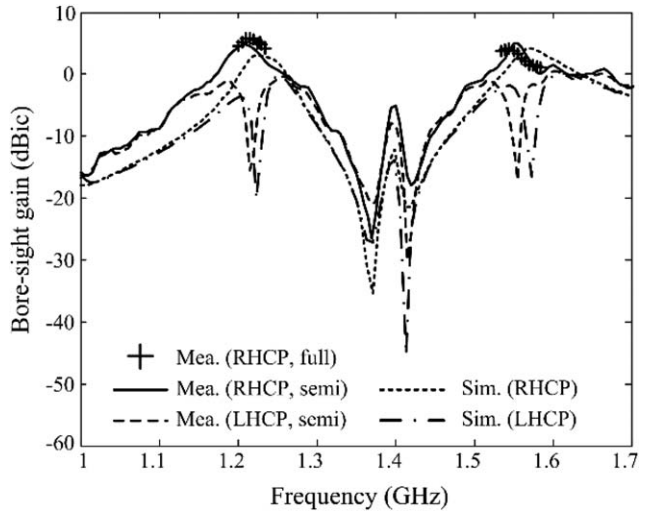

Figure 5 Bore-sight gain of the proposed antenna.

3. MEASUREMENT AND ANALYSIS

To demonstrate the capability of the dual-band polarization adjustment, we apply the proposed antenna structure for the GPS L1 and L2 bands and fabricate two antenna samples with different polarizations. The first sample has an RHC polarization with $\phi_{ar1} = 120°$ and $\phi_{ar2} = 140°$, and the geometry of the first sample antenna is asymmetric with respect to the *y*-axis, as shown in Figure 3(a). The second sample is linearly polarized with $\phi_{ar1} = 100°$ and $\phi_{ar2} = 90°$ and is symmetrical with respect to both *x*- and *y*-axes, as shown in Figure 3(b). Other design parameters of the two samples have the same values as listed in Table 1, and their antenna characteristics, such as reflection coefficients, gains, AR, and patterns, are measured in a full anechoic chamber.

Figure 4 presents a comparison of the measured and simulated reflection coefficients for the first sample antenna, which are represented by solid and dashed lines, respectively. The measured reflection coefficients are −10.2 dB and −18.1 dB at 1.575 GHz and 1.2 GHz, and the simulated values are −12.8 dB and −14.1 dB at 1.575 GHz and 1.227 GHz.

Figure 5 shows the bore-sight gain of the first sample, and measured data are specified by the solid line and '+' markers. The measured bore-sight gains are 4.2 dBic at 1.545 GHz and 5.8 dBic at 1.215 GHz, and the cross-polarization levels are −19 dB and −28.1 dB at 1.545 GHz and 1.215 GHz, respectively.

Figure 6 shows a comparison of AR values in the bore-sight direction as a function of frequency. The dashed line exhibits the simulated AR, and the measurement is expressed by '+' markers. The antenna has the minimum AR values of 1.9 dB at 1.545 GHz and 0.8 dB at 1.215 GHz for the measurement, and these values agree well with the simulated values of 1.6 dB and 1.2 dB at 1.574 GHz and 1.224 GHz, respectively.

Figures 7(a)–7(d) illustrate the measured radiation patterns of the first sample antenna in the *zx*- and *zy*-planes at 1.575 GHz and 1.227 GHz. In the upper hemisphere, its cross-polarization levels are lower than −8.8 dB and −15.9 dB in *zx*- and *zy*-planes at 1.575 GHz, respectively. At 1.227 GHz, the levels are less than −15.3 dB in *zx*-plane and −17.8 dB in *zy*-plane. The measured half-power beamwidths (HPBWs) averaged in the *zx*- and *zy*- planes are 113.4° (1.575 GHz) and 114.2° (1.227 GHz).

Figure 8 presents measured radiation patterns of the second sample antenna in comparison with the simulation. Since the antenna has linear polarization, the difference between RHC and

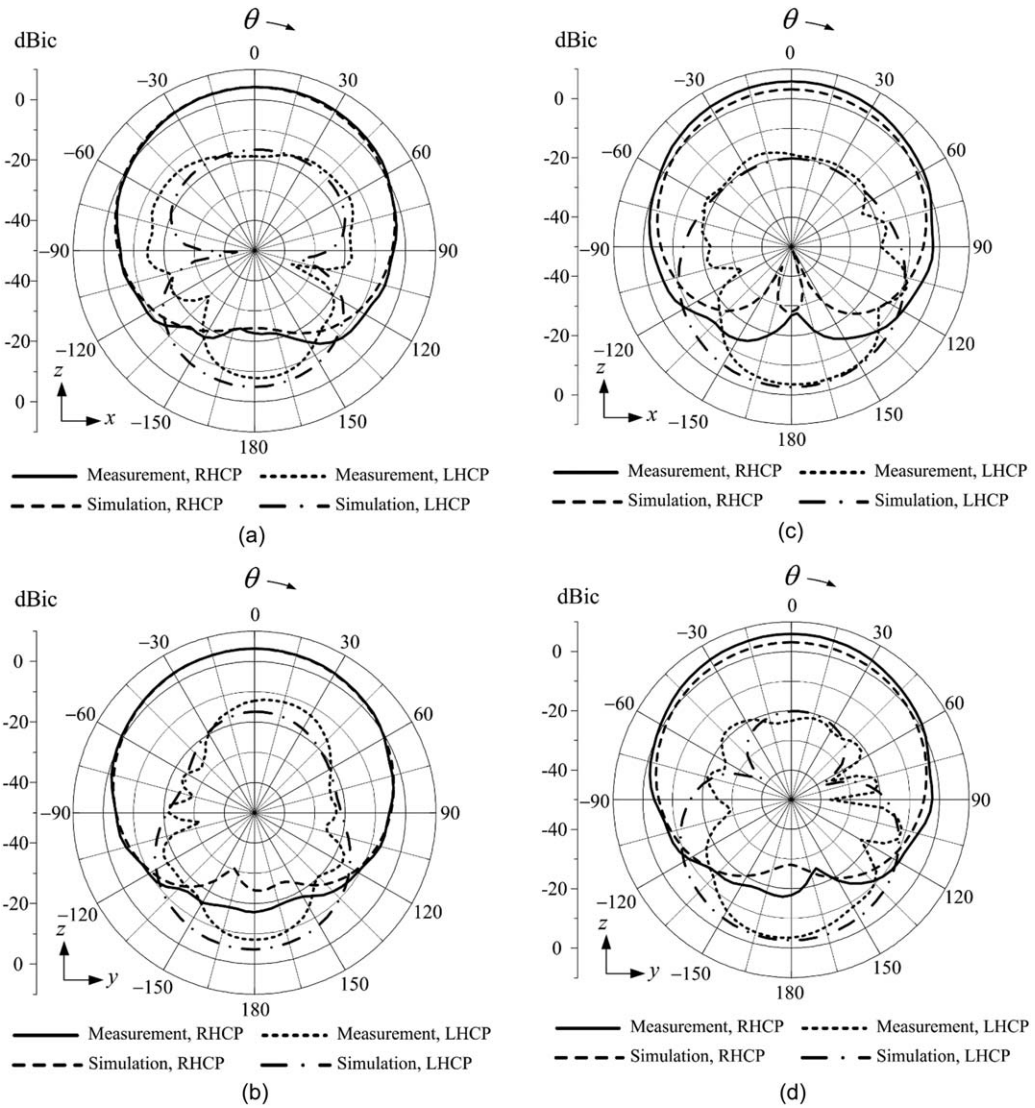

Figure 7 2-D patterns of the proposed circularly polarized antenna. (a) *zx*- plane at 1.575 GHz. (b) *zy*- plane at 1.575 GHz. (c) *zx*- plane at 1.227 GHz. (d) *zy*- plane at 1.227 GHz.

LHC gains are smaller than 2.1 dB and 6.3 dB in *zx*- and *zy*-planes at 1.575 GHz, and those at 1.227 GHz are less than 0.6 dB and 0.8 dB in the upper hemisphere. The measured HPBWs in *zx*- and *zy*-planes are 112.5° and 81.4° at 1.575 GHz and 122.8° and 115.8° at 1.227 GHz. It is important to note that the rotated parasitic elements affect only the polarization properties in the two frequency bands without degradation of other radiation characteristics, such as gain and HPBWs.

To verify how the antenna adjusts the polarization properties in the two bands, we compute H-field distributions of the first sample, as illustrated in Figures 9(a) and 9(b). The H-field strength is observed at 61 × 61 points in both the *y*- and *z*-axes, and the cross section is specified in the same figure. Figure 9(a) shows that the H-field strength is confined between the upper patch and the lower patch at 1.575 GHz with an average field strength of 11.8 A/m. On the other hand, a strong H-field distribution at 1.227 GHz is observed between the lower patch and ground with an average value of 14.4 A/m, as illustrated in Figure 9(b). These different field distributions according to the frequency enable the antenna to adjust the polarization properties independently in the two frequency bands by rotating the parasitic elements.

4. CONCLUSION

We have investigated the design of dual-band microstrip patch antennas with parasitic elements for adaptive polarization adjustments. The proposed antenna has a multi-layer structure to achieve dual-band operation, and the parasitic elements at each layer were rotated to independently adjust the antenna polarization in the two frequency bands across the entire AR range. To verify the capability of the dual-band polarization adjustment, two antenna samples with RHC and linear polarizations were fabricated, and their antenna characteristics were measured in a full anechoic chamber. The measured bore-sight gains of the circularly polarized antenna were 4.2 dBic and 5.8 dBic, and the minimum AR values were 1.9 dB and 0.8 dB at 1.545 GHz and 1.215 GHz, respectively. The cross-polarization levels of the circularly polarized antenna were smaller than −12.4 dB, on the other hand, the linearly polarized antenna showed similar gains for RHC and LHC polarizations. The results demonstrated that the proposed antenna is suitable for dual-band polarization adjustments by simply rotating the angles of the parasitic elements without any degradation of radiation gain, HPBW, and impedance matching characteristics.

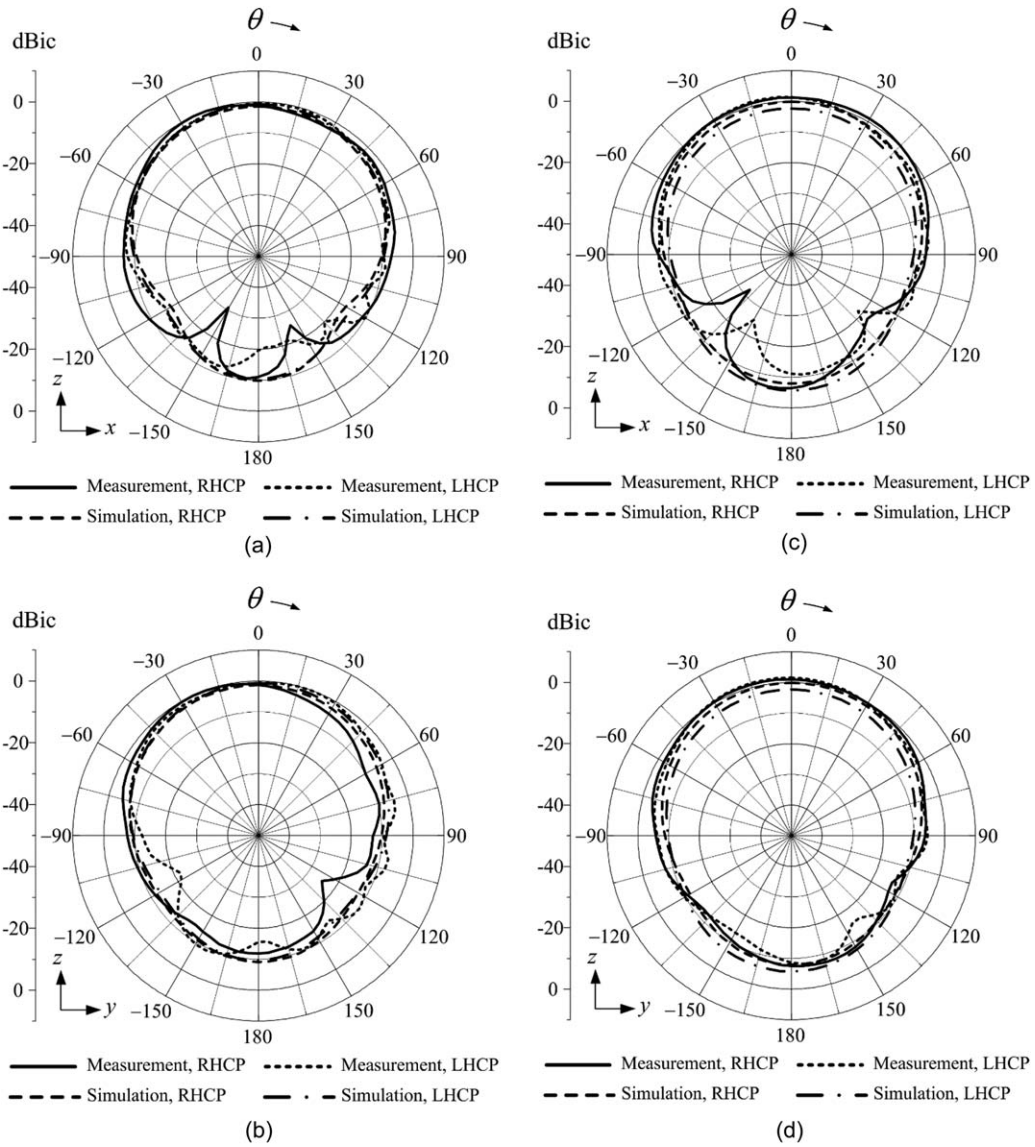

Figure 8 2-D patterns of the proposed linearly polarized antenna. (a) *zx*- plane at 1.575 GHz. (b) *zy*- plane at 1.575 GHz. (c) *zx*- plane at 1.227 GHz. (d) *zy*- plane at 1.227 GHz.

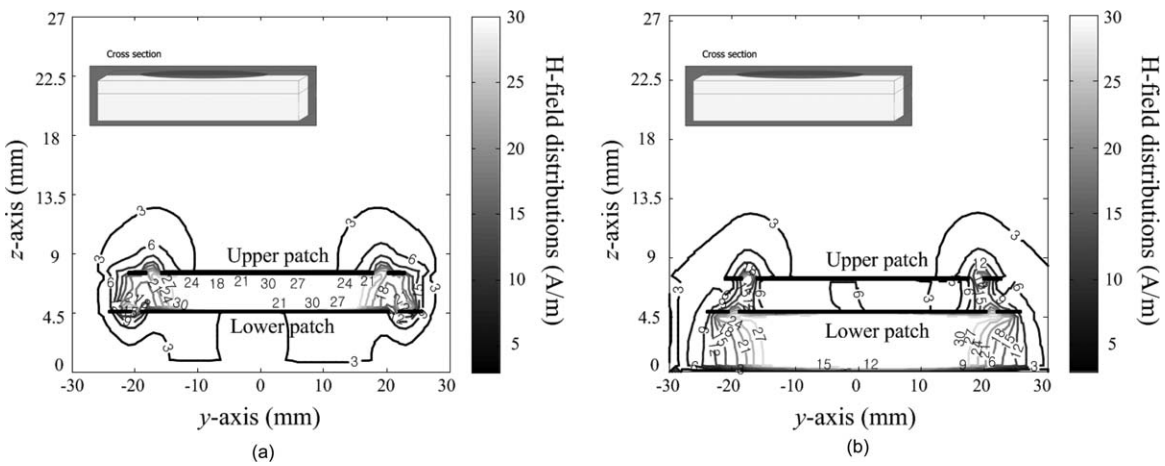

Figure 9 H-field distribution of the proposed antenna. (a) 1.575 GHz. (b) 1.227 GHz.

ACKNOWLEDGMENTS

This research was supported by Civil Military Technology Cooperation (CMTC) and the Basic Science Research Program through the National Research Foundation of Korea (NRF) funded by the Ministry of Education (No. 2015R1A6A1A03031833).

REFERENCES

1. S. Lee, J. Woo, M. Ryu, and H. Shin, Corrugated circular microstrip patch antennas for miniaturisation, Electron Lett 38 (2002), 262–263.
2. S.A. Bokhari, J.F. Zurcher, J.R. Mosig, and F.E. Gardiol, A small microistrip patch antenna with a convenient tuning option, IEEE Trans Antenna Propag 44 (1996), 1521–1528.
3. M.H. Song and J.M. Woo, Miniaturisation of microstrip patch antenna using perturbation of radiating slot, Electron Lett 39 (2003), 417–419.
4. A.M. Abbosh, Miniaturized microstrip-fed tapered-slot antenna with ultrawideband performance, IEEE Trans Antenna Wireless Propag Lett 8 (2009), 690–692.
5. J. Tang, R. Ouedraogo, E.J. Rothwell, A.R. Diaz, and K. Fuchi, A continuously tunable miniaturized patch antenna, IEEE Antenna Wireless Propag Lett 13 (2014), 1080–1083.
6. K.L. Lau, K.M. Luk, and D. Lin, A wide-band dual-polarization patch antenna with directional coupler, IEEE Antenna Wireless Propag Lett 1 (2002), 186–189.
7. C. Shichai, L. Guangcong, L. Tingfen, L. Xiangguo, and D. Zhiqi, Compact dual-band GPS microstrip antenna using multilayer LTCC substrate, Electron Lett 9 (2010), 421–423.
8. F.S. Chang, K.L. Wong, and T.W. Chiou, Low-cost broadband circularly polarized patch antenna, IEEE Trans Antenna Propag 51 (2003), 3006–3009.
9. T.N. Chang and J.M. Lin, Circularly polarized antenna having two linked slot-rings, IEEE Trans Antenna Propag 59 (2011), 3057–3060.
10. K.L. Wong and Y.F. Lin, Circularly polarised microstrip antenna with a tuning stub, Electron Lett 34 (1998), 831–832.
11. H.M. Chen and K.L. Wong, On the circular polarization operation of annular-ring microstrip patch antennas, IEEE Trans Antenna Propag 47 (1999), 1289–1292.
12. W.S. Chen, C.K. Wu, and K.L. Wong, Single-feed square-ring microstrip antenna with truncated corners for compact circular polarisation operation, Electron Lett 34 (1998), 1045–1047.
13. G. Byun, S. Kim, and H. Choo, Design of a dual-band GPS antenna using a coupled feeding structure for high isolation in a small array, Microwave Opt Technol Lett 56 (2014), 359–361.
14. G. Byun, H. Choo, and S. Kim, Design of a dual-band quadrifilar helix antenna using stepped-width arms, IEEE Trans Antenna Propag 63 (2015), 1858–1862.
15. L.I. Basilio, R.L. Chen, J.T. Williams, and D.R. Jackson, A new planar dual band GPS antenna designed for reduced susceptibility to low-angle multipath, IEEE Trans Antenna Propag 55 (2007), 2358–2366.
16. J. Tsai and J. Row, Reconfigurable square-ring microstrip antenna, IEEE Trans Antenna Propag 61 (2013), 2857–2860.
17. X.X. Yang, B.C. Shao, F. Yang, A.Z. Elsherbeni, and B. Gong, A Polarization reconfigurable patch antenna with loop slots on the ground plane, IEEE Antenna Wireless Propag Lett 11 (2012), 69–72.
18. B. Li and Q. Xue, Polarization-reconfigurable omnidirectional antenna combining dipole and loop radiators, IEEE Antenna Wireless Propag Lett 12 (2013), 1102–1105.
19. C. Sim, Y. Liao, and H. Lin, Polarization reconfigurable eccentric annular ring slot antenna design, IEEE Antenna Wireless Propag Lett 63 (2015), 4152–4155.
20. J.S. Row, W.L. Liu, and T.R. Chen, Circular polarization and polarization reconfigurable designs for annular slot antennas, IEEE Trans Antenna Propag 60 (2012), 5998–6002.
21. B. Wu, M. Okoniewski, and C. Hayden, A pneumatically controlled reconfigurable antenna with three states of polarization, IEEE Trans Antenna Propag 62 (2014), 5474–5484.
22. G. Byun and H. Choo, Antenna polarisation adjustment for microstrip patch antennas using parasitic elements, Electron Lett 51 (2015), 1046–1048.

BASE-BAND TRAINING OF CARRIER LEAKAGE CANCELLER IN 5.8-GHz FULL-DUPLEX TRANSCEIVERS

Stefano Maddio, Alessandro Cidronali, and Giovanni Collodi
Department of Information Engineering, University of Florence, V. S. Marta, Florence I-50139, Italy; Corresponding author: alessandro.cidronali@unifi.it

Received 9 April 2016

ABSTRACT: *This article introduces a training technique suitable for an active analog carrier leakage canceller, based on base-band signal processing. The proposed training approach leads to the optimum canceller parameters by observing at base-band the magnitude of a pilot signal amplitude-modulating the carrier, which is generated by the base-band processor in the transmitter and received due the leakage through the receiver chain.*

An experimental characterization applied to a road-side unit operating in full-duplex mode for an electronic toll collection system, under regulation ETSI ES200674, demonstrates that the leakage mitigation reaches up to 35 dB with the leakage between transmitter and receiver maintained below −60 dB, and resulting in a signal-noise ratio enhancement of 30 dB © 2016 Wiley Periodicals, Inc. Microwave Opt Technol Lett 58:2649–2653, 2016; View this article online at wileyonlinelibrary.com. DOI 10.1002/mop.30115

Key words: *wireless communications; leakage canceller; vehicular communications*

1. INTRODUCTION

In this article, we address the issue of radio self-interference mitigation in full-duplex transceivers suitable for Electronic Toll Collection (ETC), operating in accordance with European Telecommunications Standards Institute (ETSI) regulation. The self-interference issue affects several radio technologies, for instance frequency-division duplex communications, radio frequency identification readers [1], as well as continuous wave radar front-ends [2], to cite the most widespread. To solve this issue in a reliable and flexible way, active analog cancellation has been widely proposed in the technical and scientific literature, [3]. This class of cancelling techniques purges the leakage from the transmitter to the receiver input, by the injection of an inverted replica of the self-interfering signal itself [4]. This approach can be applied either directly at the front end [5], where the benefit is maximal but the cancellation algorithm training is difficult, or in the base-band domain [6], where the signal processing is easier, but the mitigation effect is only marginal.

In this article, we propose a technique capable of taking advantage of the benefits of these two approaches, demonstrating that an effective transmitter carrier leakage cancelling is possible, at the front-end level, having the canceller trained by measuring the signal properties at the base-band domain.

In [7,8] there were introduced a carrier leakage canceling techniques, effective in purging the leakage even when this is injected at a different section from where the canceller operates. With reference to Figure 1 this means that it is possible to operate at the section A, right before the LNA, even in the presence of leakage occurring after the canceller reference section, namely $\boldsymbol{L}2$ and $\boldsymbol{L}_3$.

In this article, we extend the above assessment by implementing a carrier side-band pilot signal in the calibration phase and moving the observation reference after the down conversion, see